A NUMERICAL STUDY OF DROPLET IMPINGEMENT FOR IN-FLIGHT ICE ACCRETION PREDICTION

Hao Zhang
Department of Mechanical Engineering, The Hong Kong Polytechnic University, Hong Kong

Chihyung Wen*
Department of Mechanical Engineering, The Hong Kong Polytechnic University, Hong Kong

Junwei Su
Department of Environment Science and Technology, Xian Jiaotong University, Xi'an, P.R.C.

ABSTRACT

Droplet impingement is the basic module in both ice accretion and anti-icing numerical calculation. A three dimensional finite volume approach with the capacity of modeling the in-flight droplet impingement on a wide range of subsonic regime is therefore established in this research, using OpenFOAM®. The Eulerian model is applied to estimate the droplet flow field with the same computational grid sets as those of the air flow calculation. The roughness effect caused by ice accretion is considered in the wall function modeling. Thus, the collection efficiency could be investigated for further icing numerical simulations. This approach is validated on both cylinder and sphere benchmark cases. The results are compared with the corresponding experimental and LEWICE (LEWis ICE accretion program) simulation data.

INTRODUCTION

In-flight ice accretion has always been a serious concern in the aeronautical engineering community. Due to weight addition and the changes of the airfoil profile the adverse effects of in-flight ice accretion on aircraft flight performance, including the availability, maneuverability, affordability, and survivability, are potential hazards to the aircraft safety. Thus, the accurate in-flight ice accretion prediction is required to develop anti-icing and de-icing technics.

Considerable researches have been done, and various approaches have been adopted in early related research, including flight test, wind tunnel experiment test, analytical and empirical approach and numerical simulation. With the qusi-steady assumption, Messinger (1953) firstly applied the conservation of energy to a control volume on the airfoil surface to investigate the ice accretion rate. This model is the foundation for all the modern icing thermodynamic models. MacArthur (1982) divided the numerical mathematic model into three interacted steps: air flow calculation, trajectory tracking for water droplets and ice accretion process with phase change, which is still adopted by most of today's icing numerical approaches.

LEWICE (developed in the United States at NASA Lewis Research Center), ONERA (developed in France at the Office National d'Études et de Recherch é Aerospatiale), and FENSAP-ICE (developed in NTI, Canada) might be today's most representative icing solvers. From 1980's, NASA started to develop LEWICE code based on the Messinger model (Ruff & Berkowitz, 1990). The prediction of LEWICE has been validated against a variety of experimental observations with adequate accuracy. LEWICE uses the three dimensional (3D) panel-method with potential flow equations to predict the air flowfield, and utilizes the Lagrangian approach with droplet motion equation to track water droplet trajectories. The above solution then be employed to compute ice accretion using the Messinger model. Other codes based on Lagrangian droplet motion models are very similar to LEWICE, such as ONERA and CANICE (developed in Canada at École Polytechnique and Bombardier).

Based on the developed Eulerian two-phase flow models, Bourgault *et al*. (1999) first proposed an Eulerian approach to numerically model the droplets impingement by using different stabilization terms. A finite element method with triangular meshes was applied to air flows containing water droplets. The calculated local collection efficiency of a simple airfoil geometry was compared with the experimental data to validate the accuracy of the model. Bourgault *et al.* (2000) developed a shallow-water thermodynamic icing model solved by a finite volume method (FVM) which combined the classical Messinger thermodynamic model and a PDEs (partial differential equations) system. Based on their work, the commercial code FENSAP-ICE (developed in NTI, Canada) was developed to

*Corresponding author: cywen@polyu.edu.hk

predict the 3D ice shapes (rime or glaze) by exploiting the same mesh. On the basis, FENSAP continuously developed serval advanced models, like models for complex geometries, de-icing model and supercooled large droplet (SLD) splashing and bouncing model.

Since in-flight ice accretion is a complicated physical process, it requires accurate and efficient numerical predictions. Droplet impingement is the important basic module to get accurate predictions in both ice accretion and anti-icing numerical calculation. Hence, this paper presents a numerical model to accurately predict the in-flight droplet impingement based on finite volume method and Eulerian two-phase model.

METHODOLOGY

A schematic plot for the basic structure of the suggested in-flight droplet impingement numerical approach is shown in Fig.1, illustrating the iterative loop of the air flow solver, droplet motion solver, and thermodynamic models solver. Coupled with the C++ package- OpenFOAM®, the numerical model integrates the 3D compressible turbulent Navier-Stokes equations, the simplified heat transfer balance at the aerodynamic surfaces and the droplet collection calculation by the Eulerian method. Details will be interpreted in the following sections.

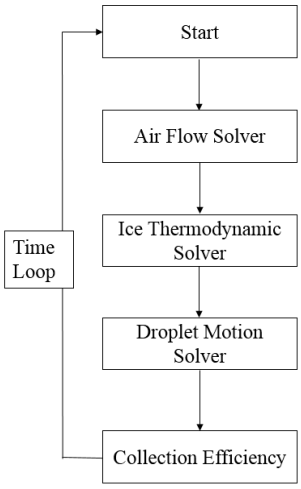

Figure 1. Schematic plot of the numerical approach of in-flight droplet impingement prediction.

Air flow solver

The formulas of the governing equations for the air flow field are defined as,

Continuity equation

$$\frac{\partial \rho}{\partial t} + \nabla \cdot (\rho \mathbf{U}) = 0 \tag{1}$$

Momentum equation

$$\frac{\partial \rho \mathbf{U}}{\partial t} + \nabla \cdot (\rho \mathbf{U}\mathbf{U}) = 0 \tag{2}$$

Energy equation

$$\begin{aligned} &\frac{\partial \rho e}{\partial t} + \nabla \cdot (\rho e \mathbf{U}) + \frac{1}{2}\frac{\partial \rho \mathbf{U}^2}{\partial t} + \frac{1}{2}\nabla \cdot \left(\rho \mathbf{U}\mathbf{U}^2\right) + \frac{\partial P}{\partial t} + \nabla \cdot (P\mathbf{U}) - P\nabla \cdot (\mathbf{U}) \\ &= -\nabla \cdot \left(\frac{2}{3}\mu(\nabla \cdot \mathbf{U})\mathbf{U}\right) + \nabla \cdot \left[\mu\left(\nabla \mathbf{U} + (\nabla \mathbf{U})^T\right) \cdot \mathbf{U}\right] + \nabla \cdot (\lambda \nabla \mathrm{T}) \end{aligned} \tag{3}$$

where ρ is the air density and $\mathbf{U}$ is the air velocity; P is the pressure and μ is the viscosity; e is the energy per unit volume and λ is the thermal conductivity.

The OpenFOAM® solver - rhoPimpleFOAM is used to solve the above equations. rhoPimpleFOAM is a transient solver with the capability to handle a wide subsonic range for laminar or turbulent compressible fluids (OpenFOAM®, 2015) and it utilizes the pressure-based PIMPLE algorithm (combination of PISO and SIMPLE algorithms).

Due to the existence of the extremely rough frozen surfaces, RANS (Reynold averaged Navier-Stokes) models commonly underestimate the convective heat flux as smooth surfaces are only considered. Thus, the thermal wall functions over rough surfaces derived by Da Silva *et al.* (2011) has been implemented in the airflow solver to investigate the roughness effects. The proposed functions are based on the model developed by the Stanford University group (Pimenta, 1975, Moffat & Kays, 1984, Kays & Crawford, 1993), described as:

$$\alpha_t = \frac{\mu_t}{Pr_t} \cdot 2 \cdot \eta \tag{4}$$

$$\eta = \frac{1}{Pr_t + \frac{\sqrt{C_f/2}}{C \cdot \left(Ks^+\right)^a \cdot Pr^b}} \tag{5}$$

where *a*, *b* and *C* are three constants respectively equal to -0.45, -0.8 and 1.42 as defined by Stefanini *et al.* (2010). C_f is the rough skin friction. $Ks^+ = U_\tau \cdot Ks/\upsilon$, Ks is the equivalent sand-grain roughness.

The limitation for the above wall functions is that the height of the first mesh must be larger than that of the roughness height, as a consequence, only high Reynolds two equation turbulence models, k-Epsilon, can be used.

The boundary conditions for the air flows are coincident with those for the corresponding IRT (icing research tunnel) experiments in NASA. And the turbulence property are determined by the property of IRT (Henze & Bragg, 1999). Two types of boundaries are mainly used: fixed values, corresponding to Dirichlet boundary condition and zero gradient, corresponding to Neuman boundary condition.

The flow field simulation results will be used to determine the water droplet motion and the convective heat transfer flux.

Droplet motion solver

Coupling with above air flow N-S equations, the Eulerian model, which is more efficient and suitable for complex in-flight models than the Lagrangian method, is proposed in this droplet solver. Assuming perfectly spherical droplets have infinite small diameter and trivial concentration in the control volume, by neglecting the effects by droplets on airflow, the splashing effect, the gravity and buoyancy force of the droplets,

the droplet-phase governing equations are expressed by a continuity equation and a momentum equation as follows:

$$\frac{\partial \alpha\rho_p}{\partial t} + \nabla\cdot\left(\alpha\rho_p \mathbf{U}_p\right) = 0 \tag{6}$$

$$\frac{\partial\left(\alpha\rho_p \mathbf{U}_p\right)}{\partial t} + \nabla\cdot\left(\alpha\rho_p \mathbf{U}_p\mathbf{U}_p\right) = F\left(\mathbf{U}-\mathbf{U}_p\right) \tag{7}$$

where α and ρ_p denotes the droplet volume fraction and the droplet density, respectively. $\mathbf{U}_p$ is the droplets velocity vector. The momentum equation ignores the viscous term and the pressure gradient while a source term of drag components caused by the air flow is added, formulated by $\alpha\rho_p \frac{f\left(Re_r\right)}{\tau_p}\left(\mathbf{U}-\mathbf{U}_p\right)$.

Where $Re_r = \frac{\left|\mathbf{U}-\mathbf{U_p}\right|\rho d_p}{\mu}$ is the Reynolds number, d_p is the droplet diameter. $\tau_p = \frac{\rho_p d_p^2}{18\mu}$ and $f\left(Re_r\right)$ could be estimated by $f\left(Re_r\right) = \frac{Re_r}{24}C_D = 1 + 0.15Re_r^{0.687} + \frac{0.0175Re_r}{1+45000Re_r^{-1.16}}$.

A concise description of the solution algorithm is proceeded in this section. The temporal and spatial discretization of the solution domain is implemented via FVM. For simplification, a general scalar transport property ϕ is used to present the droplet velocity and α, as follow,

$$\frac{\partial \phi}{\partial t} + \nabla\cdot(\mathbf{U}_p\cdot\phi) = S_\phi \tag{8}$$

where S_ϕ is source term, which is 0 for α equation. The volume integral of the above equation leads to:

$$\int_v \frac{\partial\phi}{\partial t}\cdot dv + \int_v \nabla\cdot(\mathbf{U}_p\cdot\phi)\cdot dv = \int_v S_\phi dv \tag{9}$$

Applying the divergence theorem (Gauss's law) to relate the spatial integrals to surface integrals,

$$\frac{\partial\phi}{\partial t}\cdot V + \oint_s \phi\cdot\mathbf{U}_p\cdot d\mathbf{s} = V\cdot S_\phi \tag{10}$$

The next step is the face interpolation schemes. For the droplet solver, the first order Euler scheme (for local time stepping algorithm) and the second order linearUpwind scheme are used for time derivative terms and divergence terms, respectively. Here, simple one order linear interpolation is used for the derivation, thus we have,

$$\frac{\phi_p^{n+1}-\phi_p^n}{\Delta t}\cdot V + \sum_f(\mathbf{U}_{p,f}\cdot\mathbf{S})\phi_f = V\cdot S_\phi \tag{11}$$

Let $\Psi_f = \mathbf{U}_{p,f}\cdot\mathbf{S}_f$, we have

$$\sum_f(\mathbf{U}_{p,f}\cdot\mathbf{S}_f)\cdot\phi_f = \sum_f \Psi_f\cdot[w_f\cdot\phi^{n+1} + (1-w_f)\cdot\phi_{neighbour}^{n+1}] \tag{12}$$

This can be further derived as,

$$[\frac{V}{\Delta t} + \sum_f \Psi_f\cdot w_f]\cdot\phi^{n+1} = \sum_f[-\Psi_f\cdot(1-w_f)]\cdot\phi_{neighbour}^{n+1} + \frac{V}{\Delta t}\cdot\phi_p^n + V\cdot S_\phi \tag{13}$$

$$A\cdot\phi^{n+1} = \sum_{neighbour} A_{neighbour}\cdot\phi_{neighbour}^{n+1} + B \tag{14}$$

where A, $A_{neighbour}$ and B are the corresponding matrix of Eq.(13). Then, α and $\mathbf{U}_p$ are solved sequentially and iteratively until solution converged. Figure 2 summaries the solving strategy for the droplet solver.

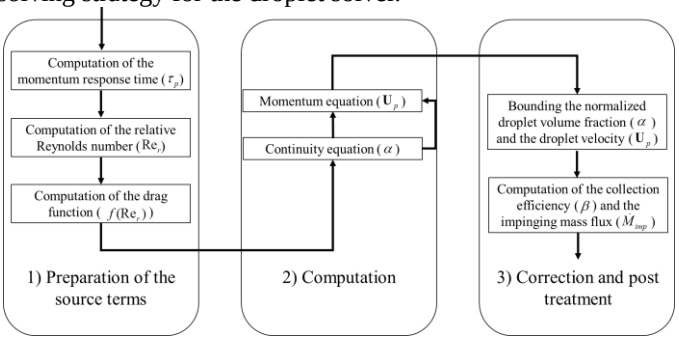

Figure 2. The solving strategy for the droplet solver.

A specific impinging boundary condition is utilized to the in-flight models to keep mass conservation in the droplet flow field. The boundary condition is required dynamical adjustment according to instantaneous directions of the local droplet. If the droplets go out of the flow field, the surface is treated as the outlet boundary, corresponding to zero gradient for the droplet volume fraction and the droplet velocity, to mimic impingement. Otherwise, droplets are blocked to go inside the flow field with the assumption of no splashing, the droplets volume fraction is assigned with a minimal value and the corresponding droplet velocity value is set to be zero.

A significant non-dimensional parameter to predict the droplet impingement is the local collection efficiency β - representing the impinging quantity of droplets, which is defined as the ratio of the water mass flux impacting a surface $\dot{M}_{imp}$ and the water mass flux in the free stream $\dot{M}_\infty$, as $\beta = \frac{\dot{M}_{imp}}{\dot{M}_\infty}$, where $\dot{M}_\infty = LWC\cdot U_\infty$, LWC is the local water content. Using the solution of droplet motion, β can be calculated by:

$$\beta = -\alpha\rho_p\frac{\mathbf{U_p}\cdot\mathbf{n}}{LWC\times U_{p\infty}} = -\frac{\alpha}{\alpha_\infty}\frac{\mathbf{U}_p\cdot\mathbf{n}}{U_{p\infty}} = -\alpha_n\frac{\mathbf{U}_p\cdot\mathbf{n}}{U_{p\infty}} \tag{15}$$

Where α_∞ and $U_{p\infty}$ is the droplet volume fraction and velocity in free stream, respectively; $\mathbf{n}$ is the surface normal to the computational domain at mesh points on solid boundaries; α_n is the normalized droplet volume fraction, defined as α/α_∞.

RESULTS & DISCUSSION

Two different benchmark cases from literatures have been investigated to validate the current numerical code, a 2D cylinder, and a full 3D sphere model, respectively.

2D cylinder validation case

The first case is 2D cylinder simulation of 4 inch diameter with 81.02 m/s free-stream velocity, corresponding to the NASA IRT experiment 091885 of Papadakis *et al.* (1989). Table 3.1 lists the setup information of the basis case, MVD is the median volume diameter of droplets.

Table 1. 2D cylinder experiment conditions

Geometry	Cylinder – 4 inches
Id	Run 091885-5C
Velocity	81.02 m/s
Pressure	95650 Pa
Density	1.185 kg/m^3
Temperature	8.2$^\circ C$
MVD	16.45μm
Reynolds number	550,000

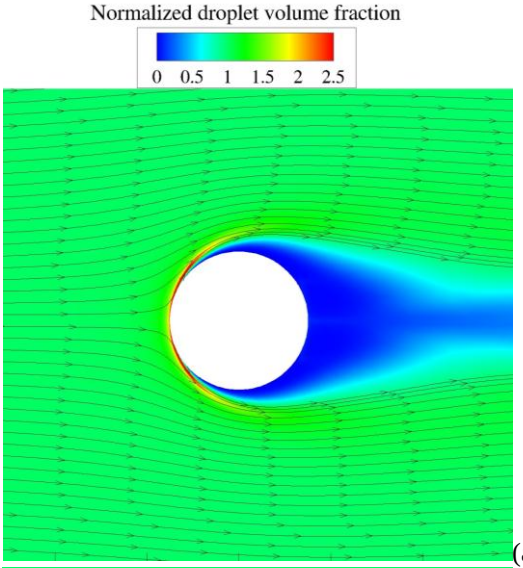

(a)

(b)

Figure 4. Normalized droplet volume fraction over a 2D cylinder with a MVD of 16.45 µm

Figure 4 shows the normalized droplet volume fraction contour with the streamlines. The streamlines of (b) go into the boundary, which demonstrates the implemented boundary condition for droplet solver functions well. Figure 5 shows the comparison of the calculated collection efficiency with the experimental data range by NASA test 091885- 6C, 6B and 5C (Papadakis *et al.*, 1989). The current result shows good agreement with the experiment range around to the stagnation point. However, the impinging area limit is under-predicted.This could be explained by the single droplet size model.

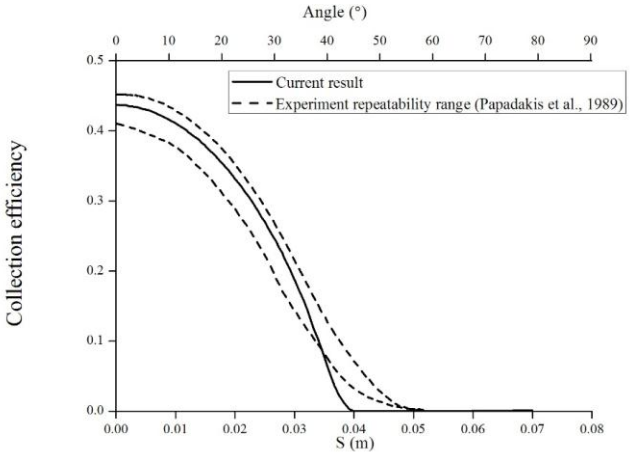

Figure 5. Comparison of predicted and experimental collection efficiency on a 2D Cylinder

3D Sphere validation case

To further validate the 3D code, we perform a 3D sphere simulation. The results are compared with the corresponding NASA IRT experimental data (Bidwell & Mohler, 1995) and with another Eulerian data (Tong & Luke, 2010). The initial conditions are given as follow:

Table 2. 3D sphere experiment conditions

Geometry	Sphere – 0.1504 m
Velocity	75.00 m/s
Pressure	95840 Pa
Density	1.192 kg/m^3
Temperature	7.0$^\circ C$
MVD	18.60μm
LWC	1.0 g/m^3
Reynolds number	760,000

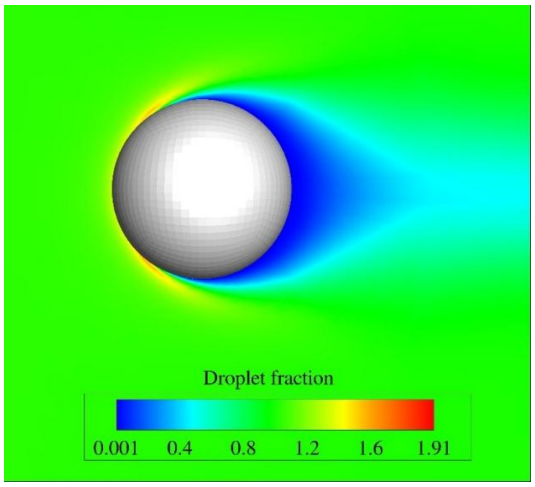

Figure 6. The volume friction contour over a 3D sphere with a MVD of 18.60μm

Figure 6 shows the volume friction contour. Compared with that of Tong & Luke (2010), the current result shows a weaker shadow area. Figure 7 shows the current results for droplets with a MVD of 18.60μm compared with the data obtained by the simulation of Tong & Luke (2010) and the experiment (Bidwell & Mohler, 1995). The two numerical simulation results are almost indistinguishable for both the collection efficiency value and the collection aera limit. Compared to the experiment, the collection area limit is underestimated in the current model as the previous 2D cylinder case. Thus, a multi-size droplet model has been considered.

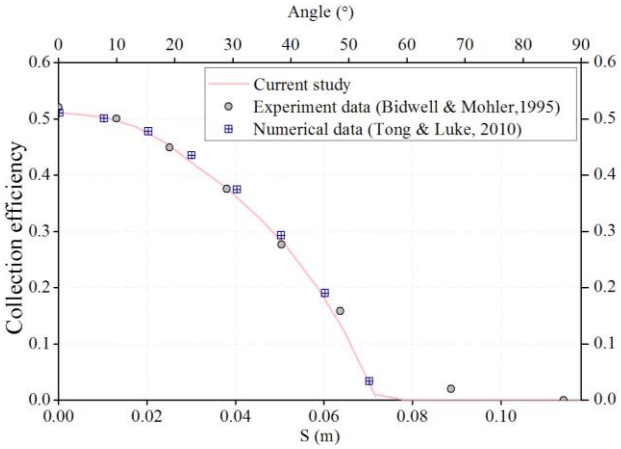

Figure 7. Comparison of the current numerical data and the reference numerical and experimental data

The same Langmuir -D distribution for the droplet sizes is selected as the experiment (Bidwell & Mohler, 1995). As shown in Fig. 8, the droplet size has a major effect on both the collection efficiency values and the collection aera limits. Figure 9 shows the droplet implingement of the muti-size model. Compared with the LEWICE data and the experimental data, the current result shows under-prediction next to the stagnation point.

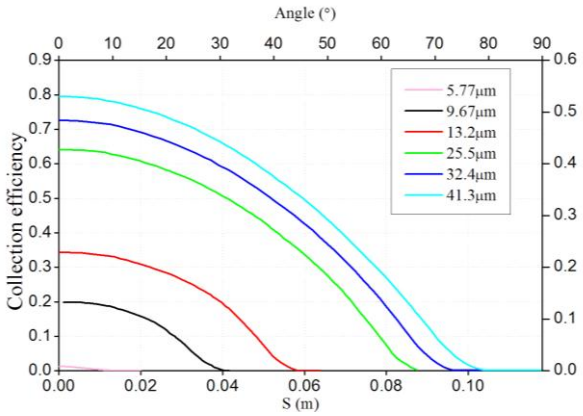

Figure 8. The collection efficiency on a 3D sphere for different droplet sizes. μ

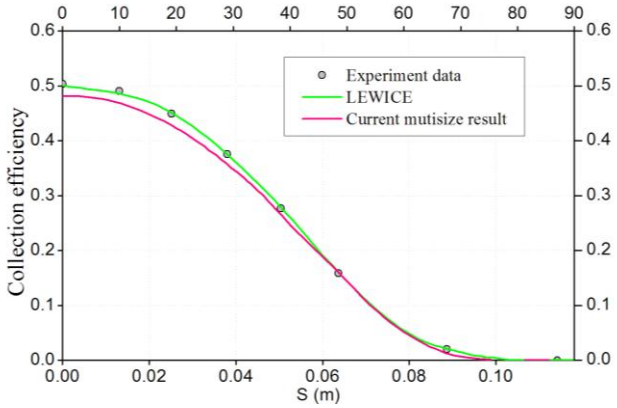

Figure 9. Comparison of current muti-size result on a 3D sphere with corresponding LEWICE and experimental data.

CONCLUSION

In this research, a 3D numerical model was established to predict in-flight droplet impingement based on the RANS unsteady finite volume air flow solver, the Eulerian two-phase model that treat the water droplet flow field as a continuum region and the simplified thermodynamic equilibrium model. The results of collection efficiency for two validation cases are in reasonably good agreement with corresponding experimental data and other numerical simulation data from the literature. The specific impinging boundary condition and the roughness wall model function effectively. Also, it is noted that the droplet size has an important effects on both the collection efficiency peak value and the collection impingement area. In the future, on the basis of this numerical model, ice accretion prediction and anti-icing/de-icing numerical code will be further developed.

REFERENCES

Bourgault, Y., Beaugendre, H., Habashi, W. Development of a shallow-water icing model in FENSAP-ICE. *Journal of Aircraft* 37, 640-646 (2000).

Bourgault, Y., Boutanios, Z., Habashi, W.G. Three-dimensional eulerian approach to droplet impingement simulation using FENSAP-ICE, Part 1: model, algorithm, and validation. *Journal of Aircraft* 37, 95-103 (2000).

Bourgault, Y., Habashi, W.G., Dompierre, J., Baruzzi, G.S. A finite element method study of Eulerian droplets impingement models. *International Journal for Numerical Methods in Fluids* 29, 429-449 (1999).

Henze, C.M., Bragg, M.B. Turbulence intensity measurement technique for use in icing wind tunnels. *Journal of Aircraft* 36, 577-583 (1999).

Kays, W.M., Crawford, M.E. Convective Heat and Mass Transfert. (1993).

Lima da Silva, G., Arima, M., Branco, N., Pimenta, M. "Proposed Wall Function Models for Heat Transfer around a Cylinder with Rough Surface in Cross Flow", *Aero-Thermal Solutions for Industry*, Brazil, (2011)

MacArthur, C.D., Keller, J.L., Luers, J.K. Mathematical modeling of ice accretion on airfoils. (*American Institute of Aeronautics and Astronautics*, 1982).

Messinger, B.L. Equilibrium temperature of an unheated icing surface as a function of air speed, *Journal of the Aeronautical Sciences*20 (1) (1953) 29–42.

Moffat, R., Kays, W. A review of turbulent-boundary-layer heat transfer research at Stanford, 1958-1983. *Advances in Heat Transfer*. 16, 241-365 (1984).

OpenFOAM® Website, www.openfoam.com

Papadakis, M., Eulangonan, R., Freund Jr., G.A., Breer, M., Zumwalt, G.W., Whitmer, L. "An Experimental Method for Measuring Water Droplet Impingement Efficiency on Two- and Three-Dimensional Bodies", *NASA Contractor Report*, USA, (1989)

Pimenta, M.M., Moffat, R.J., Kays, W.M. The turbulent boundary layer: an experimental study of the transport of momentum and heat with the effect of roughness. (*DTIC Document*, 1975).

Ruff, G.A., Berkowitz, B.M. Users manual for the NASA Lewis ice accretion prediction code (LEWICE). (1990).

Stefanini, L.M., Silvares, O.M., Silva, A.L., Zerbini, E.J.G.J. "Heat transfer on iced cylinders", *AIAA Atmospheric and Space Environments Conference*, Toronto, Canada (2010)

Tong, X., Luke, E. Robust and accurate Eulerian multiphase simulations of icing collection efficiency using singularity diffusion model. *Engineering Applications of Computational Fluid Mechanics* 4, 483-495 (2010).